# Tetracationic bis-triarylborane tetraynes as dual fluorescence and SERS sensors for DNA, RNA and proteins

Dijana Pavlović Saftić, Robert Ricker, Paul Mentzel, Johannes Krebs, Hashem Amini, Sabine Lorenzen, Nils Schopper, Adriana Kenđel, Snežana Miljanić, Jennifer Morvan, Marc Mauduit, Yann Trolez, Ivo Piantanida, Todd B. Marder

## Abstract

We report herein two new dual luminescent and Raman (SERS)-active probes, able to sense submicromolar concentrations of DNA and protein in aqueous samples. Both analogues, characterized by a tetrayne linker connecting two triarylborane fluorophores, show high binding affinities and strong fluorescent and SERS re- sponses to ds-DNA, ds-RNA, and protein (BSA). Detailed studies revealed that both the neutral and tetracationic analogue bind to ds-DNA/RNA grooves and protein (BSA) with similar affinities, at variance to previous non- charged triarylboranes, which interacted only with BSA. The fluorimetric response upon binding to BSA was different to that observed for previous analogues; the tetracationic analogue emission was enhanced and the neutral analogue emission quenched, this selectivity being attributed to the difference in solvatochromism of the triarylborane fluorophore (charged vs neutral). The neutral dye did not show any SERS signal due to the lack of interaction with negatively charged Ag nanoparticles, stressing the importance of positive charge for the application of SERS sensing. The SERS signal of the tetrayne linker of the tetracationic analogue was shifted by —81 cm—1 compared to that of the previously studied diyne analogue. The SERS signal intensity change was proportional to dye binding to ds-DNA, and completely quenched by nanomolar concentrations of BSA, such a specific response being attributed to the complete immersion of the dye within BSA.

## Keywords

Triarylborane fluorophore; DNA/RNA binding; Protein binding, fluorescent probe; SERS probe

## 1. Introduction

Probes for analytical purposes are essential for advancement in almost all fields of natural sciences. Fluorimetric sensing is by far the most intensively used method for bioimaging and biochemistry analysis [1,2]. Ḥowever, the development of novel probes has focused on a specific response to a particular target, which, in biological samples, often presents a problem due to the multitude of similar targets (pro- teins, DNA, RNA, etc.). Also, monitoring more than one dye simulta- neously often presents a considerable chalenge because of the need to add multiple external probes which have to be easily differentiated in the same sample taking into account overlapping excitation and/or emission wavelengths, possible interactions of fluorescent species, dif- ference in emission intensity, photo-sensitivity of sample, problems with auto-fluorescence of protein- and hem-containing samples, natural fluorescence of some species, and some other issues.[2].

To address this problem, other sensing methods have been intro- duced, which are complementary to fluorescence – in biomedicine, this includes PET tomography, magnetic resonance spectrometry, etc. One of the less used approaches was to develop one single reporting molecule of low molecular weight which could bind to several targets of interest with similar affinity but for each of them report by a different and complementary sensing method. We successfully applied circular di- chroism in parallel to fluorescence [3,4]; however, wavelengths of emission and induced CD response partially overlap. The Raman (SERS) method is ideal as it uses wavelengths in the infrared (IR) range, thus not overlapping with fluorescence in the visible range. Moreover, IR irra- diation has excellent living tissue penetration, allowing harmless

irradiation and collecting the response deep into the sample or even living organism. To that end, in this work, we endeavoured to combine fluorescence (the most common sensing method) with Raman (SERS) spectrometry in one reporter molecule for simultaneous detection of DNA, RNA and protein (BSA).

There have long been efforts to synthesize polyynes with different lengths and end groups, consisting of up to 44 carbon atoms linked in a row [5]. Shorter polyynes, such as diynes, triynes, and tetraynes, are a common class of natural products and are found even in vegetables, e.g., diynes in carrots, celery, and parsley, which show various biological activities [6,7]. Polyynes can potentially be applied as pharmaceuticals [8] or functional materials [9]. They can serve as molecular wires [10,11] or as a component of dyes, such as the red-emitting tetrayne in Scheme 1a, reported by Tang and coworkers, which can be used for cancer cell imaging [12,13]. However, the main remaining challenges for the application of polyynes are selective synthesis and purification [14].

To synthesize polyynes with even numbers of ethyne units (e.g., diynes and tetraynes), which bear the same end-cap on both sides, the copper-catalyzed oxidative Glaser, Hay, and Eglinton coupling reactions are commonly used [15–17]. The oxidative dimerization of terminal acetylenes can also be conducted in a co-catalyzed manner, using palladium and copper catalysts [18]. When the target polyynes bear two different end-caps or contain an uneven number of ethyne units, they can be obtained via the Cadiot-Chodkiewitz reaction, the Fritsch–Buttenberg–Wiechell rearrangement, or *via* molybdenum- catalyzed alkyne metathesis [19–22]. The end-capping of polyynes with bulky groups contributes to their stability [23–26]. Polyynes end- capped with hydrogen (*terminal*) or halogens can be extremely reac- tive or prone to explosion, and have caused injuries and damage in laboratories in the past [27,28]. The possibilities for further function- alization of polyynes are broad. For example, they can be catalytically hydrogenated, borylated [29], serve as precursors for metallacycles [30] and σ-polyyne complexes [31], or be utilized in cyclization reactions [14].

Triarylboranes have been explored with regard to their synthetic access and optical properties, enabling their potential application in dyes, sensors, and optoelectronic materials [32–37]. Their most prom- inent properties are based on the empty p-orbital on the boron center, which leads to strong π-electron acceptor ability when connected to a π-system, enabling the design of charge-transfer compounds [38,39]. Triarylboranes can become water-soluble when substituted with trimethylammonium groups at the *para*-position of the aryl rings, and water-stable, when the central boron atom is protected with at least five *o*-methyl groups [40–42]. Alkynylated triarylboranes have previously been incorporated in several materials such as BODIPY-dyes, rhenium acetylide complexes used as chemosensors, and in platinum acetylide complexes for optical power limiting [43–45]. Our group recently studied applications of triarylboranes in cell imaging [34,42,43,47,48] and the interaction of rod-like triarylborane compounds with DNAs and RNAs [42,46,47]. Small molecules can interact with DNA/RNA via external binding, intercalation, and groove binding, with the latter typically taking place for the systems we reported [48]. We recently reported a tetracationic bis-triarylborane 1,3-butadiyne chromophore (**24**+, Scheme 1b) [15], which interacts with DNA/RNA and proteins and can be probed *via* fluorescence and surface-enhanced Raman spectroscopy (SERS) [49,50]. The polyyne motif was selected as a linker in our current research, as polyynes are excellent Raman probes. The motif has even been used for spectral barcoding, as Raman absorption is distinctively influenced by the substitution pattern and length of the polyyne chain [51].

Based on our recent work on bis-triarylborane-diyne dyes, we extended the polyyne system to prepare the analogous tetrayne (Scheme 1c); as Raman intensity rises exponentially with the length of the conjugated alkyne system, a longer linker can result in a better and more sensitive imaging dye [52]. We also expected to achieve more effective groove binding in ds-DNA/RNA by increasing the distance between the bulky triarylborane moieties.

## 2. Materials and methods

Unless otherwise noted, all reactions were performed using standard Schlenk or glovebox (Innovative Technology Inc.) techniques under argon. Reagent grade solvents were argon saturated, dried using an Innovative Technology Inc. Pure-Solv Solvent Purification System, and further deoxygenated by using the freeze–pump–thaw method. All starting materials were purchased from commercial sources and used without further purification. Automated flash chromatography was performed using a Biotage® Isolera Four system on silica gel or NH-silica, GC–MS analyses were performed using an Agilent 7890A gas

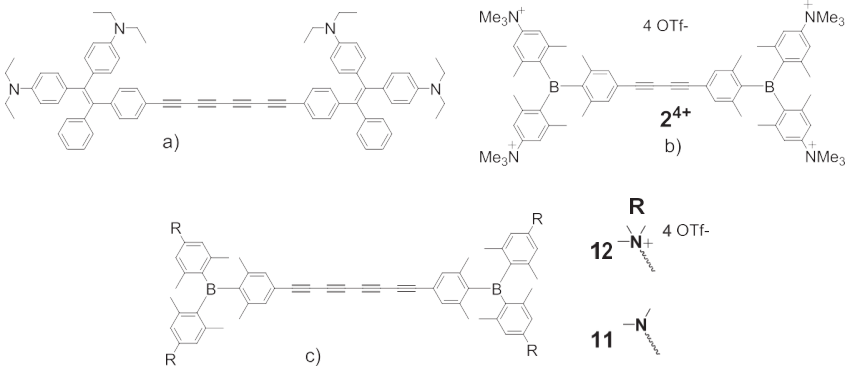


**Scheme 1.** a) Example of a red-emitting tetrayne dye reported by Tang and coworkers.12b) Recently developed tetracationic triarylborane-diyne dye 24 groups for DNA/RNA/BSA dual-method sensing via SERS and fluorescence [64], c) Novel bis(triarylborane) tetrayne analogues studied in this work.

+ by our

chromatograph, high-resolution mass spectrometry was obtained using a Thermo Scientific Exactive Plus MS System. The NMR spectra were recorded at ambient temperature on a Bruker DRX-300, Bruker Avance 500 NMR or Bruker Avance Neo I 600 NMR.

Full experimental details for the synthetic procedures are provided in the Supporting Information.

*2.1. Crystal structures*

Deposition number 2250177 (for **11**) contains the supplementary crystallographic data for this paper. These data are provided free of charge by the joint Cambridge Crystallographic Data Centre and Fachinformationszentrum Karlsruhe Access Structures service.

*2.2. Study of interactions with DNA, RNA, and BSA*

The solvents, sodium cacodylate buffer ( = 0.05 M, pH = 7.0), dimethyl sulfoxide (DMSO, Alfa Aesar), and toluene (Sigma-Aldrich) were used without further purification.

Polynucleotides were purchased as noted: poly A–poly U (Sigma), calf thymus (*ct*)-DNA (Aldrich) and dissolved in sodium cacodylate buffer ($I$ = 0.05 M, pH = 7.0). The *ct*-DNA was additionally sonicated and filtered through a 0.45 μm filter to obtain mostly short (ca. 100 base pairs) rod-like B-helical DNA fragments. Polynucleotide concentrations were determined spectroscopically as the concentration of phosphates (corresponds to *c*(nucleobase)).

All measurements of interactions with ds-DNA/RNA were performed in aqueous buffer solution (pH = 7.0, sodium cacodylate buffer, $I$ = 0.05 M). The UV–Vis spectra were recorded on a Varian Cary 100 Bio spectrometer, fluorescence spectra were recorded on a Varian Cary Eclipse fluorimeter, and CD spectra were recorded on a JASCO J815 spectropolarimeter at 25.0 ◦ C, equipped with a thermostatting device, using appropriate quartz cuvettes (Hellma Suprasil QX, path length 1 cm).

The absorption spectral changes of **11** and **12** were recorded upon stepwise addition of DNA/RNA or BSA stock solutions into the cuvette. The absorbances were sampled at 1 nm intervals, with an integration time of 10 s.

Fluorimetric titrations at $\lambda$exc were performed by adding aliquots of a polynucleotide or BSA stock solutions to a solution of the compound. The UV and fluorimetric data obtained were corrected for the dilution and used for the calculation of binding constants by fitting to the dye/BSA 1:1 stoichiometry of the complex formed.

Thermal melting curves for ds-DNA, ds-RNA, and their complexes with the compounds studied were determined as previously described [64], by monitoring the absorption change at 260 nm as a function of temperature. The absorbance of the ligands was subtracted from every curve, and the absorbance scale was normalized. $T$m values are the midpoints of the transition curves determined from the maximum of the first derivative and checked graphically by the tangent method [53]. The Δ$T$m values were calculated by subtracting the $T$m of the free nucleic acid from the $T$m of the complex. Every Δ$T$m value here reported was the average of at least two measurements. The error in Δ$T$m is ± 0.5 C◦. CD experiments were performed by adding portions of the compound stock solution into the solution of the polynucleotide. The spectra were recorded as an average of three accumulations with a scan speed of 200 nm/min and a buffer background was subtracted from each spectrum.

*2.3. SERS analysis*

*2.3.1. General information*

SERS spectra upon excitation at 1064 nm were measured using a Bruker Equinox 55 interferometer equipped with FRA 106/S Raman module and Nd-YAG laser of 500 mW power. Quartz cuvettes with a back-placed mirror were used for handling colloidal samples. The spectra were recorded in the 3500–100 cm—1 spectral range at a resolution of 4 cm—1 and averaged over 128 scans.

A Renishaw inVia Raman microscope was used for measurements of SERS spectra upon excitation at 785 nm. Laser radiation of 15 mW power was focused on the colloidal sample placed in a 40-μL aluminium pan using a 5 × microscopic objective (NA = 0.12). The spectra were recorded in the 3200–100 cm—1 spectral range at a resolution of 1 cm—1 with an exposure time of 10 s.

*2.3.2. Metal substrate synthesis*

The colloidal suspension of silver nanoparticles was prepared by the reduction of silver nitrate with trisodium citrate using the modified Lee and Meisel method [54].The UV/Vis absorption maximum of the silver colloid was 412 nm, and the pH value of the colloidal suspension was 6.9. The suspension of silver nanoparticles prepared was centrifuged at 5000 rpm for 15 min. The supernatant (85 % of the initial colloidal suspension) was removed, and the residue containing silver nano- particles (15 % volume of the initial colloidal suspension) was used as the SERS substrate.

*2.4. Biology*

*2.4.1.Cells*

A549 (human lung carcinoma; ATCC CCL-185) were obtained from the ATCC Cell Biology Collection and were cultured according to the manufacturer's instructions. Cells were grown in Dulbecco Modified Eagle's Medium (DMEM, Sigma Aldrich, USA) supplemented with 10 % of fetal bovine serum (FBS, Sigma Aldrich, USA) at 37 ◦ C and 5 % CO2 in a humidified atmosphere. Three biological replicas were performed for all experiments.

*2.4.2. Cytotoxicity assay – MTT*

[55] The compounds studied were dissolved in an appropriate volume of dimethyl sulfoxide (DMSO) under sterile conditions, to obtain 10 mM stock solutions, and were kept in the dark at + 4 ◦ C. Before each assay, fresh working solutions were prepared from the stock solution by diluting them with DMEM. Cells were seeded on 96 well plates at concentrations of 7 x 103 cells/well in 100 μL of DMEM (10 % FBS) and left in the incubator overnight (37 ◦ C, 5 % CO2). The next day, 100 μL of the working solution was added to the wells, thus the final volume was 200 μL/well. All measurements were made in quadruplicate. Cells treated with the same dilutions of DMSO represented the control, while cells treated only with DMEM (10 % FBS) represented the negative control. The plate was then incubated for the next 72 h (37 ◦ C, 5 % CO2). After incubation, the medium was removed, and 40 μL of an MTT solution was added to each well. The plate was incubated in the cell incubator for 3 h, allowing formazan crystals to form. After 3 h, 170 μL of DMSO was added to each well and the plate was placed on a shaker for 20 min, allowing the crystals to dissolve. The absorbance of the MTT-formazan product was measured with a microplate reader at 600 nm, and the absorbance value correlates directly with cell survival.

## 3. Results and discussion

*3.1. Synthesis*

Starting compound **8** was prepared by previously reported protocols [15] (Supp. Info. Scheme SI-3). To obtain 1,3-butadiyne **9**, a modified, stepwise Cadiot-Chodkiewicz protocol was used, because the electrophilic alkyne reagent (bromoethynyl)trimethylsilane would decompose under normal one-step Cadiot-Chodkiewicz conditions. In the first step, terminal alkyne **8** was deprotonated by *n*BuLi, followed by treatment with 1.1 eq. of CuI to form the copper acetylide, which was not isolated. The Cu-acetylide was then reacted with (bromoethynyl)trimethylsilane to give **9** (Scheme 2). Another possible route, starting from the brominated triarylborane alkyne was not feasible, as the bromination of **8** could not be achieved selectively using NBS. Alkaline deprotection of **9** gave the terminal 1,3-butadiyne derivative **10**, which is quite unstable,

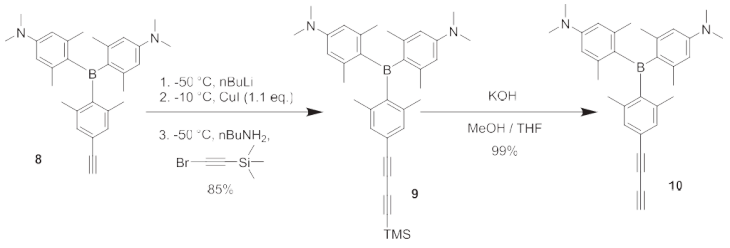


**Scheme 2.** Stepwise Cadiot-Chodkiewicz-coupling to form **9**, followed by alkaline deprotection to obtain **10**.

and was stored at —30 ◦ C or used immediately after preparation.

In a Pd/Cu co-catalyzed Glaser-type reaction, **10** was then homo- coupled yielding tetrayne **11.** To obtain a water-soluble dye, **11** was then methylated at all four nitrogens, to give the triflate salt **12**. (Scheme 3). Full details of the characterization of the compounds are provided in the Supporting Information.

In addition to the diyne already reported [15] and the tetrayne described above, we attempted to synthesize the corresponding triyne (Scheme 4, Supp. Info. Scheme S4). We thus used our recent methodology based on alkyne metathesis, [22] which requires an unsymmetrical diyne containing a bulky group on one end and a non-hindered group on the other end. We hypothesized that the triarylylboron group of compound **9** could provide sufficient steric hindrance to prevent the adjacent C≡C bond from reacting, knowing that the trimethylsilyl (TMS) group was small enough [56]. Therefore, compound **9** was reacted with the Fürstner catalyst **Mo-1** [57] in toluene at room temperature for 4 h. However, no trace of the expected triyne was observed. Instead, diyne **14** was isolated in 53 % yield (entry 1) [58]. As we suspected that the TMS group was in fact too large to allow discrimination between the two C≡C bonds, the diyne **10** was then investigated. Unfortunately, no conversion was observed, and only the starting material was recovered (entry 2). This agrees with the fact that some Mo-catalysts are poisoned by terminal C≡C bonds [59]. In a last attempt, we used compound **13** which contains two diynes linked by an alkyl chain instead of a TMS or H end group. After reaction under the same conditions, only diyne **14** was isolated in 43 % yield, but again no triyne was detected (entry 3). We conclude that the triarylylboron group was not bulky enough to prevent the adjacent C≡C bond from reacting. Thus, unfortunately, we were not successful in synthesizing the triyne analogue of **11**.

### *3.2. Single-crystal X-ray diffraction*

The molecular structure of compound **11** was obtained by single-crystal X-ray diffraction (Fig. 1).

The alkyne rods display a parallel staggered orientation (see Supporting Information, Fig. S1). The distance between the rods is 4.444(2) Å, whereby they are kept apart by the bulky end-caps. The length of the chain, measured between the two boron atoms, is 20.382(2) Å, while the rod is slightly bent in an S-shape with a variation of 176.12(14) ◦ — 177.73(16) ◦ for the C — C — C angles. The dihedral angle between the two aryl rings attached to the tetrayne rod is 74.46(4) ◦ .

Compared to our previous molecular modelling results with close analogues of **11** and **12** and biorelevant targets [47,48], the structure of **11** in solid state retained rod-like structure, which fitted well into ds-DNA/RNA grooves, thus suggesting that novel compounds **11** and **12** could retain a similar binding mode and affinity toward ds-DNA/RNA.

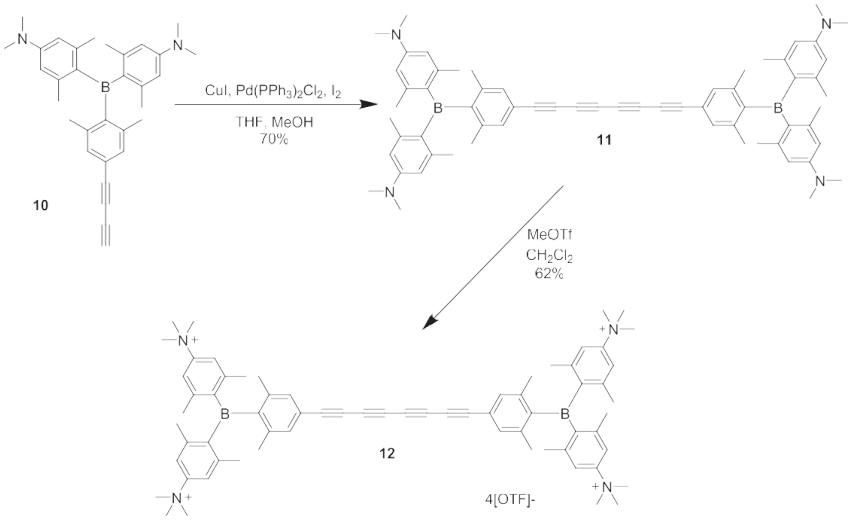


**Scheme 3.** Oxidative Cu/Pd-catalyzed diyne homo-coupling to give tetrayne **11**,and subsequent methylation yielding the triflate salt **12.**

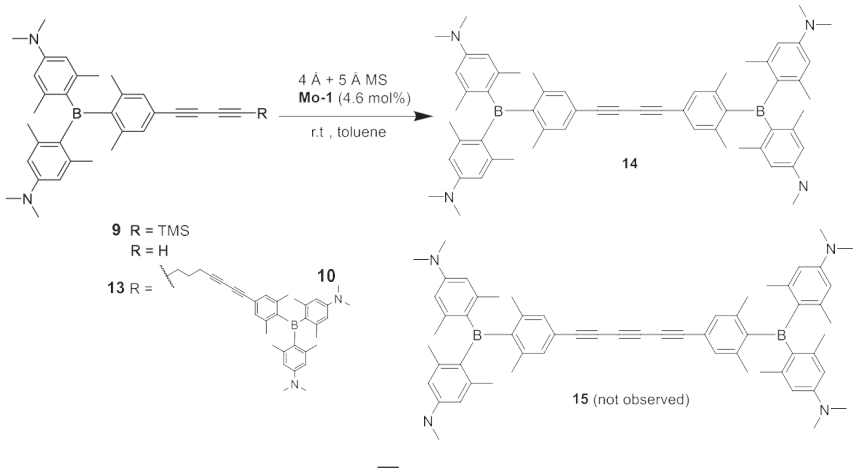


| Entry | Substrate | Conv. (4 h) | Yield diyne 14 (%) |
|---|---|---|---|
| 1 | **9** | 55 | 53 |
| 2 | **10** | 0 | - |
| 3 | **13** | 45 | 44 |

Alkyne metathesis of diynes **9, 10,** and **13** with **Mo-1** (**Mo-1** = (Ph3SiO)3Mo(CC-C6H4-4-OMe)).
**Scheme 4.**

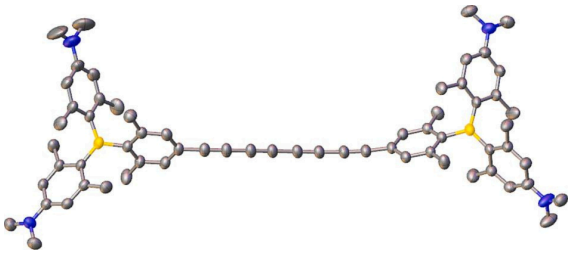

**Fig. 1.** Molecular structure of **11** in the solid state with thermal ellipsoids drawn at the 50% probability level. Hydrogen atoms are omitted for clarity. Atom colours: carbon (grey), boron (yellow), nitrogen (blue).

Moreover, for the very close diyne analogue **24+** (Scheme 1b) the orientation of such a rod-like structure controlled the intensity of the SERS signal and also its sensitivity to the sensing of biotargets [15], thus the tetrayne presented herein could show enhanced sensing ability.

### *3.3. Photophysical properties*

The linear optical properties of **11** and **12** were investigated in solution (Fig. 2 and Table 1). Both compounds absorb in the UV and to ca. 475 nm in the visible region of the spectrum and the absorption is barely affected by the solvent polarity. The emission spectra of neutral tetrayne **11** are broad and featureless, being dominated by characteristic local charge-transfer bands, arising from the NMe2-arene-B moieties. The emission spectrum of **12** shows a vibronic fine structure, along with a reduced quantum yield. Compound **11** exhibits a solvatochromic emission redshift of 3825 cm—1 from toluene to diethyl ether solutions, while for **12** the emission redshift from EtOH to water is only 410 cm—1, as methylation of the amines shuts off the charge-transfer process.

Due to its poor solubility in water, a stock solution of **11** was prepared in DMSO at *c* = 0.005 M and diluted in buffered aqueous solution

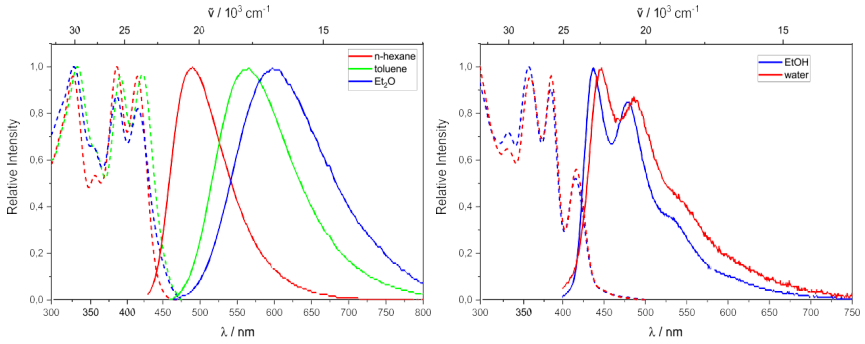


**Fig. 2.** Normalized absorption (dashed) and emission (solid) spectra of **11** in n-hexane, toluene, and diethyl ether solutions (left) and of **12** in ethanol and water solution (right).

**Table 1**
Photophysical data of **11** and **12** solutions in solvents of different polarity.

| # | Solvent | [a]ε ($M^{-1}cm^{-1}$) | λmax abs (nm) | λmax em (nm) | Stokes shift ($cm^{-1}$) | Φ | τ (ns) | $\tau^0$ (ns) | $k_{nr}/10^7 s^{-1}$ | $k_r/10^7 s^{-1}$ |
|---|---|---|---|---|---|---|---|---|---|---|
| **11** | n-hexane | – | 329<br>388<br>416 | 488 | 3500 | 0.09 | 1.27 | 14.1 | 71.7 | 7.1 |
| **11** | toluene | 56,000 | 335<br>393<br>423 | 563 | 5900 | 0.12 | 3.96 | 33.0 | 22.2 | 3.0 |
| **11** | Et2O | – | 330<br>387<br>416 | 600 | 7400 | 0.07 | 2.15 | 30.7 | 43.3 | 3.3 |
| **12** | EtOH | – | 359<br>385<br>415 | 438<br>478<br>530 | 1300 | 0.02 | 0.69 | 34.5 | 142.0 | 2.9 |
| **12** | water | 47,000 | 359<br>385<br>415 | 446<br>487<br>540 | 1700 | 0.01 | 1.24 | 124.0 | 79.8 | 0.8 |

[a] Molar extinction coefficients were determined at the absorption band of the lowest energy.

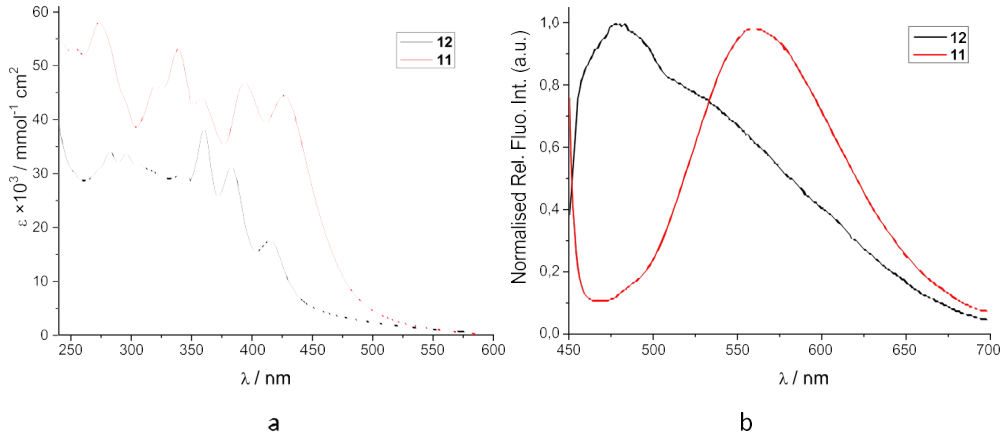


**Fig. 3.** a) UV/Vis spectra; b) Fluorescence spectra, **11** ($c = 3.51 \times 10^{-7}$ M, $\lambda^{exc} = 420$ nm), **12** ($c = 5 \times 10^{-7}$ M, $\lambda^{exc} = 415$ nm), normalized to their emission maxima. Done at pH 7.0, sodium cacodylate buffer, $I = 0.05$ M.

in further experiments, whereby the absorbance was proportional to concentration up to c = 2 × 10—5 M (Supp. Info., Fig S3). The stock solution of tetracationic **12** was prepared in water at *c* = 0.01 M. Solutions of the compounds, stored at + 8 ◦ C, were stable for at least one week. Changes in the UV/Vis spectra of **11** and **12** were negligible upon temperature increase up to 95 ◦ C. The UV/vis spectra of the aqueous solutions of **11** and **12** differ (Fig. 3A), with the absorption of neutral **11** being shifted bathochromically, similarly to the fluorescence emission (Fig. 3B). Both compounds' fluorescence intensities are proportional to concentration up to c = 2 × 10—6 M, showing negligible changes with temperature. All results indicate that the compounds do not aggregate by intermolecular stacking under the experimental conditions employed.

### *3.4. Interactions with ds-DNA, ds-RNA and BSA*

As previously studied triarylborane analogues15,42,47,48 showed intriguing biorelevant interactions and, being strong chromophores and fluorophores, act as probes for various DNA/RNA sequences and proteins, we studied the interactions of derivatives **11** and **12** with the most commonly used ds-DNA representatives, namely naturally isolated calf thymus (ct)-DNA, the most commonly used synthetic ds-RNA representative, poly A – poly U, as well as synthetic ss-RNAs consisting of common four nucleobases (poly, A, poly G, poly C, poly U). For a model protein, we used bovine serum albumin, BSA.

The addition of ds-DNA resulted in a moderate hypochromic effect in the UV/Vis spectra of **11** and **12** (Supp. Info., Fig. S4) and, for **12**, a pronounced bathochromic shift was observed. However, small changes and insufficient solubility of the compounds did not allow accurate calculation of the binding constants.

The intrinsic fluorescence of **11** and **12** was strongly quenched by the addition of any ds-DNA or ds-RNA (Fig. 4, Supp. Info. Figs S5–S6). The addition of ss-RNAs also quenched the emission of **11** (Supp. Info. Figs S7–S10) but in most cases resulted in precipitation of **12**, likely due to the neutralisation of ss-RNA negative charge by tetracationic **12**. Most fluorimetric titrations allowed the processing of the data by the Scatchard equation [60] to obtain the binding constants (Table 2).

The addition of BSA resulted in opposite changes in the fluorescence of the compounds studied fluorescence; the emission of **11** was quenched and that of **12** was strongly increased (Fig. 5). This behaviour can be correlated with the strong solvatochromism of the neutral

**Table 2**

Bindingconstants (log *Ks*)a calculated from the fluorescence titrations of **11** and **12** withctDNA, ds-RNA (pApU), ss-RNAs and BSA at pH 7.0 (buffer sodium cacodylate, *I* = 0.05 M).

| | *ct*-DNA | pApU | pA | pG | pC | pU | BSA |
|---|---|---|---|---|---|---|---|
| **11** | 8.1 | 8.0 | 6.0 | 6.6 | 6.4 | 6.5 | 7.4 |
| **12** | 8.4 | 8.1 | [b] | 6.4 | [b] | [b] | 7.1 |
| [c]**24**$^+$ | 6.9 | 7.6 | 7.2 | 7.5 | 7.4 | 6.7 | 8.2 |

[a] Titration data with DNA or RNA were processed according to the Scatchard equation,61 with the correlation coefficient R > 0.999, the best fit obtained for ratio n[dye]/[polynucleotide] = 0.1–0.3, for better comparison all data re-fitted to n = 0.2; for ss-RNA, the best fit obtained for ratio n[dye]/[polynucleotide] = 0.4–0.7, for better comparison all data re-fitted to n = 0.5; and titration with BSA was fitted to the 1:1 stoichiometry of dye/BSA complex. bPrecipitation. cPublished results.15.

analogue **11** (as shown in Fig. 2, left) at variance with the negligible changes observed for tetracationic **12** (Fig. 2, right). Obviously, these fluorophores respond very differently to changes in their solvation shell, which occurs upon insertion of a molecule in the deep, strongly hydrophobic binding site inside BSA.

Detailed analysis of binding constants (Table 2) revealed that **11** and **12** have similar, 5–10 nM affinity toward ds-DNA/RNA, which is order of magnitude stronger in comparison to dyne analogue (**24**+, Scheme 1)15 whereas affinity relation toward BSA is opposite: **24**+ binding stronger than tetraynes **11** or **12**. Thus, the length of the "-yne" linker directly controls the binding selectivity ratio between ds-DNA/RNA and protein (BSA), in a way that a shorter linker better fits into the BSA binding site, whereas a longer linker accommodates within DNA/RNA groove with more flexibility, allowing stronger interactions of triarylborane ends with DNA/RNA backbone.

Surprisingly, neutral analogue **11** showed to be a more applicable dye for ss-RNAs than tetracationic analogue **12**, later causing precipitation of its complex with ss-RNA due to the neutralization of the anionic RNA backbone by four positive charges of the triarylborane end-groups. However, the affinity of **11** or **12** toward ss-RNA was an order of magnitude weaker in comparison to shorter dyne analogue **24**+. Since ss-RNA do not have a well-defined secondary structure, available experimental data do not allow the accurate explanation of difference in binding constants, thus supporting future studies of the most promising analogue **11** with short RNA oligonucleotides by NMR techniques.

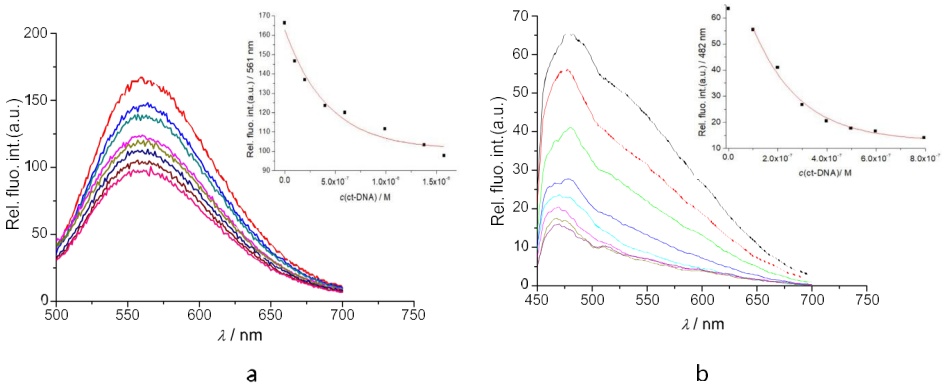


**Fig. 4.** a) Changes in fluorescence spectrum of **11** (*c* = 3.5 ×10—7 M, λexc = 420 nm) upon titration with ctDNA, Inset: Dependence of emission at λmax = 561 nm on c (ctDNA) fitted to the Scatchard equation; b) Changes in fluorescence spectrum of **12** (*c* = 5 ×10—7 M, λexc = 415 nm) upon titration with ctDNA, Inset: Dependence of emission at λmax = 482 nm on *c*(ctDNA) fitted to the Scatchard equation Done at pH 7.0, sodium cacodylate buffer, *I* = 0.05 M.

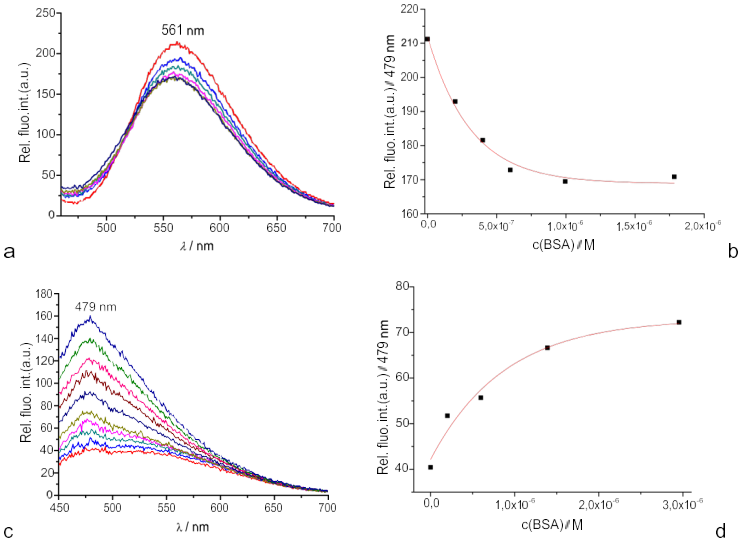


**Fig. 5.** a) Changes in the fluorescence spectrum of **11** (c = 5 × 10—7 M, λexc = 420 nm) upon titration with BSA; b) Dependence of **11** emission at λmax = 561 nm on c (BSA); (bottom left); c) changes in fluorescence spectrum of **12** (c = 5 × 10—7 M, λexc = 415 nm) upon titration with BSA; d) Dependence of **12** emission at λmax = 479 nm on c(BSA) Done at pH 7.0, sodium cacodylate buffer, *I* = 0.05 M.

### *3.5. Circular dichroism (CD) experiments*

To obtain insight into the changes in polynucleotide properties induced by small molecule binding, we employed CD spectroscopy as a highly sensitive method to observe conformational changes in the sec- ondary structure of polynucleotides [61]. In addition, achiral small molecules **11** and **12** can acquire induced CD (ICD) upon binding to polynucleotides, which could provide useful information about modes of interaction [62].

The addition of tetracationic **12** caused only a moderate decrease in ds-DNA/RNA CD spectra and no measurable ICD bands (Fig. 6), suggesting only a minor decrease of ds-polynucleotide chirality, as a consequence of the partial unwinding of the double helix. Similar effects observed for both ds-DNA and ds-RNA suggested that **12** is predominantly binding within the hydrophobic grooves of the polynucleotides, whereby the absence of ICD bands at > 300 nm could be attributed to the non-uniform orientation of chromophores within binding sites.63 Addition of the neutral compound **11** resulted in a similar but less

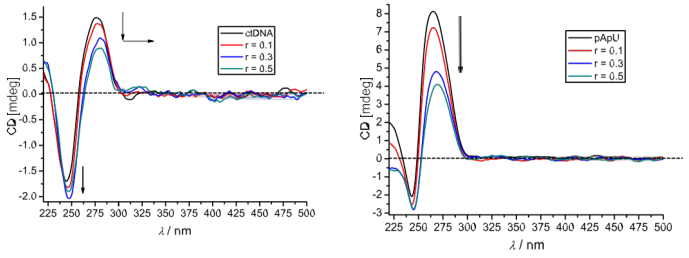


**Fig. 6.** CD titration of ctDNA (c = 3 ×10—5 M) and poly A – poly U (c = 3 ×10—5 M) with **12** at molar ratios r = [compound] / [polynucleotide] (pH 7.0, buffer sodium cacodylate, I = 0.05 M).

pronounced effect (Supp. Info., Fig. S11), likely due to the binding within similar binding sites, but with no electrostatic contribution (which is present in tetracationic **12**). These CD results, along with the observed strong binding affinity of **11** and **12** to DNA/RNA (Table 2) and thermal stabilization effects (Table 3), support binding into ds-DNA minor or ds-RNA major groove, as demonstrated previously for our other triarylborane chromophores.15,47,48

### *3.6. Thermal denaturation experiments*

Thermally-induced dissociation of the ds-polynucleotides into two single-stranded polynucleotides occurs at a well-defined temperature (Tm value), this property being quite sensitive to the small molecule binding. Non-covalent binding of small molecules to ds-polynucleotides usually increases the thermal stability of the ds-helices, thus resulting in an increased *T*m value, and this increase (Δ*T*m) can (in corroboration with other methods) be related to the various binding modes [63]. In our previous studies, cationic triarylboranes usually strongly stabilized ds-DNA or ds-RNA; thus, we performed experiments with **11** and **12**.

Similar to previous analogues15 (Scheme 1, 24+), the addition of **11** or **12** at saturation ratio r[dye]/[polynucleotide] = 0.3 resulted in precipitation of dye/polynucleotide complex, thus hampering the determination of Δ*T*m values. Presuming that neutralization of the DNA/RNA negative charge by the dye could be the reason for precipitation, we performed experiments at low ratios r = 0.05 and 0.1 (Supp. Info., Fig. S12 and S13), at which homogeneous solutions of the complex were preserved.

The results (Table 3) revealed that the neutral compound **11** does not stabilize double-stranded DNA or RNA against thermal denaturation, in line with previously studied neutral triarylboranes,15 whereas tetracationic **12** showed moderate stabilization of ds-DNA/RNA, comparable to its diyne analogue15 **24**+.

### *3.7. Raman/SERS studies*

We have recently reported several groups of bis-triarylborane fluorophores equipped with either diyne or aryl-diyne linkers, which acted as simultaneous Raman (SERS) and fluorescence probes.47,15 Thus, the tetrayne bis-triarylboranes **11** and **12** were studied under comparable conditions.

A silver colloid for SERS measurements was prepared using a previously described protocol.47,15 Due to the low solubility of **11** in water, working samples for concentration-dependent SERS measurements were prepared by dissolution of a stock solution of **11** ($c$ = 1 × 10—4 M in DMSO) in an appropriate volume of DMSO, followed by the addition of the silver colloid. The DMSO volume ratio ($v/v$) was 20 % in the samples prepared, and the final concentrations of **11** were 5 × 10—6 M and 1 × 10—5 M.

The SERS spectra of non-charged **11** in the silver colloidal suspension resembled the SERS spectrum of pure DMSO (Supp. Info., Fig. S14), and the observed vibrational bands corresponded to vibrational modes of DMSO (Supp. Info., Table S1). The lack of SERS bands for **11** was attributed to the absence of interactions with the metallic surface. Most likely, the neutral **11** molecules were not able to adsorb onto the metal surface due to negatively charged citrate ions surrounding the silver nanoparticles.

In contrast to non-charged **11**, tetracationic **12** showed a pronounced SERS spectrum, stressing the importance of positive charge for the binding to the negatively charged Ag nanoparticles' surface. The concentration-dependent SERS spectra of **12** ($c$ = 1 × 10—7 M, 5 × 10—7 M, 1 × 10—6 M, 5 × 10—6 M and 1 × 10—5 M), obtained upon excitation at both 785 nm and 1064 nm (Fig. 7, A and B), allowed the assignment of the SERS bands (Table 4). In addition to attractive electrostatic interactions, a band at ca. 225 cm—1, assigned to Ag — N stretching, indicated the chemical bonding of the molecules studied with the silver surface. Despite NIR excitation, a raised baseline was observed in the SERS spectra as the result of the fluorescence of **12**.

In the SERS spectrum of **12**, a band at ca. 2130 cm—1 is assigned to the stretching of the triple C≡C bond, while a band at 1592 cm—1 (at 1598 cm—1 upon 785 nm excitation) is attributed to a phenyl stretching mode in the triphenyl borane units. The bands at 1256 and 1133 cm—1 (1264 and 1139 cm—1 upon 785 nm excitation) originate from the phenyl vibrational modes, while a band at ca. 1090 cm—1 is associated with the stretching of the bonds between the boron atom and the phenyl rings. The most intense SERS spectrum of **12** was obtained at a concentration of 5 × 10—6 M. At this concentration, **12** molecules were most likely perpendicularly oriented towards the metal surface when the scattered radiation was most enhanced. A decrease in **12** concentration was followed by a diminution in the intensity of the characteristic **12** bands, pointing to a detection limit of 5 × 10—7 M.

As both ct-DNA and BSA were prepared in Na-cacodylate buffer, the effect of the buffer on the SERS spectrum of **12** was investigated (data not shown). An increased baseline was obtained in the spectra of the buffered samples upon excitation at 785 nm as well as at 1064 nm, most likely due to aggregation of Ag nanoparticles induced by ions in the buffer solution. However, new bands were not observed, and the position of the existing ones did not change after adding the buffer to the sample.

Comparison of data for **12** with previously studied diyne analogues15 collected at comparable conditions (laser excitation 758 nm) revealed two distinctive differences in the signal attributed to the C≡C triple bond. The tetrayne band maximum at 2134 cm—1 is shifted by 81 cm—1 to lower energy with respect to the diyne band at 2215 cm—1, agreeing well with analogous systems under biorelevant conditions.52 However, the lowest detection limit of the diyne signal at 2215 cm—1 (5 × 10—8 M)15 is superior to the lowest detection limit of the tetrayne signal at 2134 cm—1 (5 × 10—7 M). Thus, simple multiplying of triple bonds does not lead to a proportional increase of the SERS signal.

As only the tetracationic derivative **12** showed SERS spectrum, we studied the impact of DNA or BSA addition with this molecule only. Samples of **12**/ct-DNA complexes were prepared by mixing the compound with ct-DNA resulting in **12**/ct-DNA molar ratios of 1/1, 1/3, 1/5, 1/10, ($c$(**12**) = 5 × 10–6 M).

In the SERS spectra of **12**/ct-DNA complexes (Fig. 8), the baseline was increased due to dye fluorescence; however, it decreased with higher contents of DNA in the complex. Bands characteristic of **12** were obtained in the spectra of the complexes at compound/ct-DNA molar ratios of 1/1 and 1/3, whereas at compound/ct-DNA molar ratios of 1/5 and 1/10, the spectra corresponded to the spectrum of the colloid.

The SERS spectra of **12**/BSA complexes at the molar ratios of 1/1, 1/5 and 1/10 were measured, ($c$(**12**) = 5 × 10–6 M). Unlike the complexes with ct-DNA, the addition of even the smallest amount of BSA completely quenched the SERS spectra of **12** (Supp Info, Fig. S15). Such an effect was also observed in our previous studies and was attributed to the binding of **12** deep into the binding pocket of BSA,47,15 thus completely removing the dye from the Ag nanoparticles' surface.

**Table 3**
$\Delta T_m$-Valuesa (∘ C) for different ratios b of sample added to ctDNA or poly A – poly U.

| Compound | *r* | ct-DNA | poly A –poly U |
|---|---|---|---|
| **11** | 0.05 | +0.8 | +0.3 |
| | 0.1 | 0 | +0.5 |
| **12** | 0.05 | +1.2 | +1.1 |
| | 0.1 | +2.3 | +3.1 |
| c**24**+ | 0.1 | +4.0 | – |

a Error in ΔTm: ± 0.5 ∘ C;

b *r* = [compound] / [polynucleotide].

c Published results15.

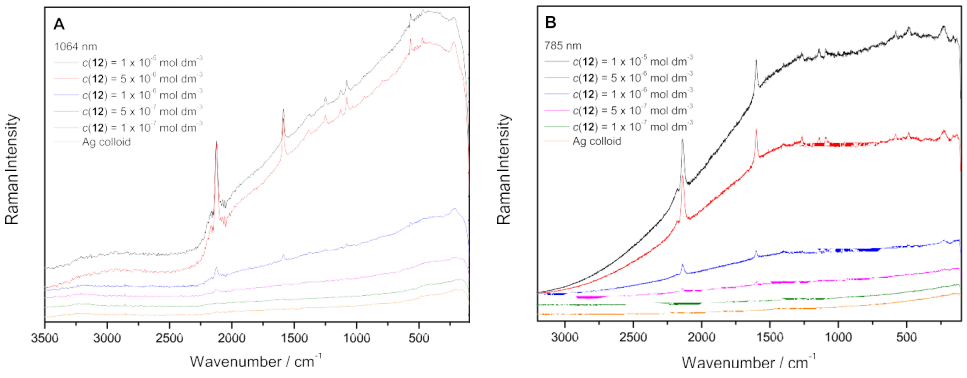


**Fig. 7.** Raman spectra of the silver colloid (orange) and concentration-dependent SERS spectra of **12** ($c$ = 1–––100 × 10— displaced for visual clarity. A) Excitation wavelength $\lambda$ex = 1064 nm, laser power 500 mW; B) Excitation wavelength $\lambda$ ex = 785 nm, laser power 15 mW.

[7] M) in the silver colloid. The spectra are

**Table 4**
Assignment of the SERS bands in the spectrum of **12,** c = 5 ×10—6 M.

| Wavenumber / cm— [1] | | Assignment |
|---|---|---|
| λex = 1064 nm | λex = 785 nm | |
| 2127 | 2134 | ν C≡C |
| 1592 | 1598 | ν CC (phenyl) |
| 1256 | 1264 | δip CH (phenyl) |
| 1133 | 1139 | δip CH (phenyl) |
| 1084 | 1090 | ν B—(Car)3 |
| 574 | 578 | CC (phenyl) |
| 226 | 229 | δ Ag — N |
| | | ν |

*3.8. Biological studies*

Prior experiments in this work showed that **11** and **12** strongly bind to ds-DNA/RNA, which, if it happens in the cells, can cause strong cytotoxicity.49 To study the cytotoxic effect of compounds **11** and **12**, the human lung carcinoma cell line (A549) was treated with 10 μM, 1 μM and 0,1μM solutions of the corresponding compounds, and cell survival was assessed by the MTT assay,56 whereby in comparison to the control cells (not treated by compound), the compounds showed negligible toxicity (Fig. 9).

Based on the similar non-toxicity of previously studied analogues, in future research compounds **11** and **12** could be safely used as cellular probes – to that goal, detailed biological studies, beyond the scope of this chemistry-focusedwork, are in progress.

## 4. Conclusions

Newly prepared bis-triarylborane dyes linked by tetraynes were synthesized in both, neutral and tetracationic form. Both molecules are moderately fluorescent in solution and exhibit characteristic alkyne stretching absorptions in their IR and Raman spectra.

The tetracationic derivative **12** binds with submicromolar affinity to ds-DNA or ds-RNA within the DNA/RNA grooves, somewhat stronger in comparison to previously studied cationic triarylboranes.15 In contrast to previously studied neutral triarylboranes, neutral analogue **11** also interacted with ds-DNA/RNA. Both compounds bind strongly to ss-RNA, particularly neutral **11** showing a strong emission response.

The addition of BSA caused an opposite effect on the fluorescence of the chromophores; the emission of neutral **11** was quenched and that of

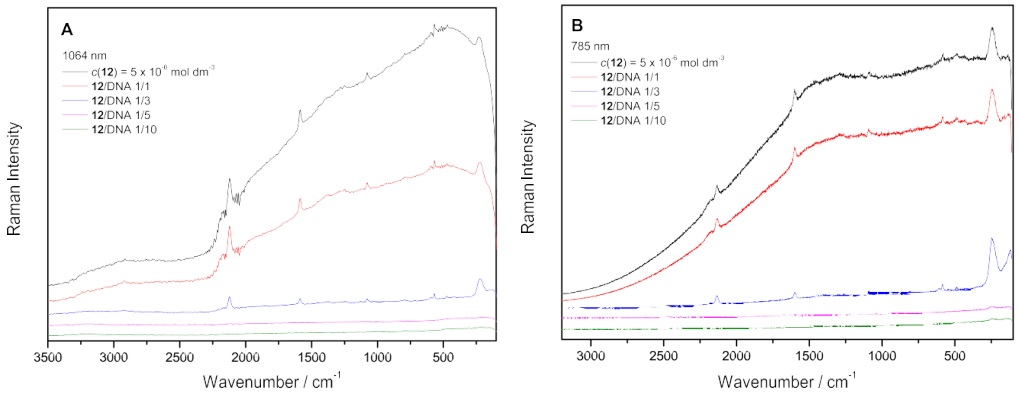


**Fig. 8.** SERS spectra of **12** in Na-cacodylate buffer, pH 7.0, (black); the ratio of **12**/ct-DNA is depicted in the figure. The spectra are displaced for visual clarity. A) Excitation wavelength $\lambda_{ex}$ = 1064 nm, laser power 500 mW; B) Excitation wavelength λex = 785 nm, laser power 15 mW.

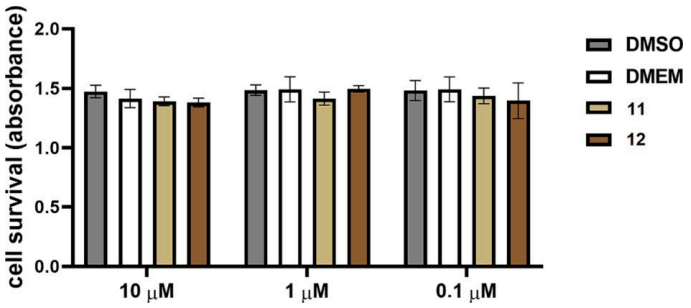


**Fig. 9.** Cell survival of A549 cells treated with different concentrations of **11** and **12**. Data are presented as mean ± SD made in four replicates, relative to the control samples. Control samples are cells treated with DMSO at the same concentration as the compound being tested. Representative data from two independent biological replicas which yielded similar results are shown.

cationic **12** was strongly increased. Such a selective response was attributed to the very different electronic properties of fluorophores and resulting solvatochromic response, thus finely sensing the change in solvation shell upon insertion of molecule in the deep, strongly hydrophobic binding site inside BSA.

Thus, tetracationic derivative **12** is an excellent fluorimetric probe for distinguishing between DNA/RNA (quenching) and for BSA (strong increase).

Both compounds exhibit Raman spectra in the solid state; however, upon the addition of a silver colloid, only the tetrayne linker of tetracationic **12** showed a measurable SERS spectrum at submicromolar concentrations, in contrast to neutral **11**. This result stressed the importance of electrostatic interactions between the positively charged small molecule and the negatively charged citrate layer on the silver colloid, which is essential to the uniform orientation of small molecules in a favorable position to obtain a SERS signal. Comparison with previously studied diyne analogues15 revealed a tetrayne band with a maximum at 2134 cm—1 shifted by —81 cm—1 with respect to the analogous diyne, in agreement with analogous systems under biorelevant conditions.52 However, the ~ 20 % loss of intensity compared to the diyne analogue15 points out that simply multiplying the number of triple bonds does not lead to a proportional increase in the SERS signal. Therefore, our recently reported alternative route of introducing an aromatic moiety in the center of the diyne linker,47 which actually increased the lowest detection limit to nanomolar concentrations, is a far more promising route for the design of novel fluorescent/Raman probes.

The SERS signal intensity was proportional to **12** binding to ds-DNA and was completely quenched by the smallest amount of BSA, such a specific response being attributed to the complete immersion of the dye within BSA, thus losing contact with silver colloid.

Both new dyes did not show any cytotoxicity in human cell lines and therefore can be applied as safe probes for *in vitro* studies. Thus, tetracationic probe **12** yields the opposite and specific response for ds-DNA/RNA/ss-RNA in comparison to protein BSA, in both, fluorescence and SERS signal. These results strongly support further research of DNA/RNA/protein targeting fluorescence/Raman (SERS) probes and encourage the development of analytical protocols in biorelevant conditions, including sensing inside living cells (new compounds being non-toxic).

## References

[1] R.B. Silverman, *The organic chemistry of drug design and drug action*, 2nd edn.,, Elsevier Academic Press, Amsterdam, 2004.

[2] M.-A. Mycek, B.W. Pogue. Handbook of Biomedical Fluorescence, CRC Press, Boca Raton, USA, 2003.

[3] J. Gershberg, M. Radi´c Stojkovi´c, M. Skugor, S. Tomic, T.H. Rehm, S. Rehm, C. R. Saha-Moller, I. Piantanida, F. Wurthner, Sensing of double-stranded dna/rna secondary structures by water soluble homochiral perylene bisimide dyes, Chem. Eur. J. 21 (2015) 7886–7895, https://doi.org/10.1002/chem.201500184.

[4] L.M. Tumir, I. Crnolatac, T. Deligeorgiev, A. Vasilev, S. Kaloyanova, M. G. Branilovic, S. Tomic, I. Piantanida, Kinetic differentiation between homo- and alternating at dna by sterically restricted phosphonium dyes, Chem. Eur. J. 18 (2012) 3859–3864, https://doi.org/10.1002/chem.201102968.

[5] W.A. Chalifoux, R.R. Tykwinski, Synthesis of polyynes to model the sp-carbon allotrope carbyne, Nat. Chem. 2 (2010) 967–971, https://doi.org/10.1038/nchem.828.

[6] A.L. Shi Shun, R.R. Tykwinski, Synthesis of naturally occurring polyynes, Angew. Chem. Int. Ed. 45 (2006) 1034–1057, https://doi.org/10.1002/anie.200502071.

[7] C. Zidorn, K. Jo¨hrer, M. Ganzera, B. Schubert, E.M. Sigmund, J. Mader, R. Greil, E. P. Ellmerer, H. Stuppner, Polyacetylenes from the Apiaceae vegetables carrot, celery, fennel, parsley, and parsnip and their cytotoxic activities, J. Agric. Food Chem. 53 (2005) 2518–2523, https://doi.org/10.1021/jf048041s.

[8] Y. Pan, T.L. Lowary, R.R. Tykwinski, Naturally occurring and synthetic polyyne glycosides, Can. J. Chem. 87 (2009) 1565–1582, https://doi.org/10.1139/V09-117.

[9] M.R. Bryce, A review of functional linear carbon chains (oligoynes, polyynes, cumulenes) and their applications as molecular wires in molecular electronics and optoelectronics, J. Mater. Chem. C 9 (2021) 10524–10546, https://doi.org/10.1039/D1TC01406D.

[10] C.S. Casari, M. Tommasini, R.R. Tykwinski, A. Milani, Carbon-atom wires: 1-D systems with tunable properties, Nanoscale 8 (2016) 4414–4435, https://doi.org/10.1039/C5NR06175J.

[11] C. Thiele, L. Gerhard, T.R. Eaton, D.M. Torres, M. Mayor, W. Wulfhekel, H.V. Lo¨hneysen, M. Lukas, STM study of oligo(phenylene-ethynylene)s. New. J. Phys. 17 (2015) 053043. https://doi.org/10.1088/1367-2630/17/5/053043.

[12] Z. Zhao, H. Su, P. Zhang, Y. Cai, R.T. Kwok, Y. Chen, Z. He, X. Gu, X. He, H.H. Sung, Polyyne bridged AIE luminogens with red emission: design, synthesis, properties

and applications, J. Mater. Chem. B 5 (2017) 1650–1657, https://doi.org/10.1039/C7TB00112F.

[13] F. Cataldo, Polyynes: synthesis, properties, and applications, CRC Press, Boca Raton, 2005.

[14] B. Pigulski, N. Gulia, S. Szafert, Reactivity of polyynes: complex molecules from simple carbon rods, Eur. J. Org. Chem. 2019 (2019) 1420–1445, https://doi.org/10.1002/ejoc.201801350.

[15] R. Akhtar, A.F. Zahoor, Transition metal catalyzed Glaser and Glaser-Hay coupling reactions: scope, classical/green methodologies and synthetic applications, Synth. Commun. (2020) 1–32, https://doi.org/10.1080/00397911.2020.1802757.

[16] I. Deperasin´ska, A. Szemik-Hojniak, K. Osowska, M. Rode, A. Szczepanik, T. Lis, S. Szafert, Synthesis, photophysics and excited state structure of 1,8-di (p-tolyl)-1,3,5,7-octatetrayne, J Photochem. Photobiol. 217 (2011) 299–307, https://doi.org/10.1016/j.jphotochem.2010.10.023.

[17] N. Gulia, K. Osowska, B. Pigulski, T. Lis, Z. Galewski, S. Szafert, Mori-Hiyama versus Hay coupling for higher polyynes, Eur. J. Org. Chem. 2012 (2012) 4819–4830, https://doi.org/10.1002/ejoc.201200554.

[18] A.S. Batsanov, J.C. Collings, I.J. Fairlamb, J.P. Holland, J.A. Howard, Z. Lin, T. B. Marder, A.C. Parsons, R.M. Ward, J. Zhu, Requirement for an oxidant in Pd/Cu co-catalyzed terminal alkyne homocoupling to give symmetrical 1,4-disubstituted 1,3-diynes, J. Org. Chem. 70 (2005) 703–706, https://doi.org/10.1021/ jo048428u.

[19] S. Radhika, N.A. Harry, M. Neetha, G. Anilkumar, Recent trends and applications of the Cadiot-Chodkiewicz reaction, Org. Biomol. Chem. 17 (2019) 9081–9094, https://doi.org/10.1039/C9OB01757G.

[20] T. Luu, Y. Morisaki, N. Cunningham, R.R. Tykwinski, One-pot formation and derivatization of di- and triynes based on the Fritsch—Buttenberg—Wiechell rearrangement, J. Org. Chem. 72 (2007) 9622–9629, https://doi.org/10.1021/jo701810g.

[21] I. Curbet, S. Colombel-Rouen, R. Manguin, A. Clermont, A. Quelhas, D.S. Müller, T. Roisnel, O. Basl´e, Y. Trolez, M. Mauduit, Expedient synthesis of conjugated triynes via alkyne metathesis, Chem. Sci. 11 (2020) 4934–4938, https://doi.org/10.1039/D0SC01124J.

[22] S. Eisler, N. Chahal, R. McDonald, R.R. Tykwinski, Alkyne migration in alkylidene carbenoid species: A new method of polyyne synthesis, Chem. Eur. J. 9 (2003) 2542–2550, https://doi.org/10.1002/chem.200204584.

[23] M. Springborg, L. Kavan, On the stability of polyyne, Chem. Phys. 168 (1992) 249–258, https://doi.org/10.1016/0301-0104(92)87159-7.

[24] F. Cataldo, Stability of polyynes in air and their degradation by ozonolysis, Polym. Degrad. Stab. 91 (2006) 317–323, https://doi.org/10.1016/j.polymdegradstab.2005.04.046.

[25] M. Gulcur, P. Moreno-García, X. Zhao, M. Baghernejad, A.S. Batsanov, W. Hong, M. R. Bryce, T. Wandlowski, The Synthesis of Functionalised Diaryltetraynes and Their Transport Properties in Single-Molecule Junctions, Chem. Eur. J. 20 (2014) 4653–4660, https://doi.org/10.1002/chem.201304671.

[26] T. Gibtner, F. Hampel, J.P. Gisselbrecht, A. Hirsch, End-cap stabilized oligoynes: model compounds for the linear sp carbon allotrope carbyne, Chem. Eur. J. 8 (2002) 408–432. https://doi.org/10.1002/1521-3765(20020118)8:2<408::AID-CHEM408>3.0.CO;2-L.

[27] A. Glen, S. Hutchinson, Contribution of triacetylene to the biological effects of Fomes annosus, Trans. Brit. Mycol. Soc. 61 (1973) 583–585, https://doi.org/10.1016/S0007-1536(73)80127-5.

[28] R.H. Baughman, Dangerously seeking linear carbon, Science 312 (2006) 1009–1110, https://doi.org/10.1126/science.1125999.

[29] a) G. Lesley, P. Nguyen, N.J. Taylor, T.B. Marder, A.J. Scott, W. Clegg, N.C. Norman, Synthesis and Characterization of Platinum(II)—Bis(boryl) Catalyst Precursors for Diboration of Alkynes and Diynes: Molecular Structures of cis-[(PPh)2Pt(B-4-But cat)2], cis-[(PPh3)2Pt(Bcat)2], cis-[(dppe)Pt(Bcat)2], cis-[(dppb)Pt(Bcat)2], (E)-(4-MeOC6H4)C(Bcat)CH(Bcat), (Z)-(C6H5)C(Bcat)C(C6H5)(Bcat), and (Z,Z)-(4-MeOC6H4)C(Bcat)C(Bcat)C(Bcat)C(4-MeOC6H4)(Bcat) (cat = 1,2-O2C6H4; dppe = Ph2PCH2CH2PPh2; dppb = Ph2P(CH2)4PPh2), Organometallics 15 (1996) 5137–5154. https://doi.org/10.1021/om950918c b) S. Jos, C. Szwetkowski, C. Slebodnick, R. Ricker, K.L. Chan, W.C. Chan, U. Radius, Z. Lin, T. B. Marder, W.L. Santos, Transition Metal-Free Regio- and Stereo-Selective trans Hydroboration of 1,3-Diynes: A Phosphine-Catalyzed Access to (E)-1-Boryl-1,3-Enynes. Chem. Eur. J. 28, e202202349. https://doi.org/10.1002/chem.202202349 c) J. Szyling, A. Szyman´ska, A. Franczyk, J. Walkowiak, [Pt(PPh3)4]-Catalyzed Selective Diboration of Symmetrical and Unsymmetrical 1,3-Diynes, J. Org. Chem. 87 (2022) 10651–10663. https://doi.org/10.1021/acs.joc.2c00844.

[30] a) C. Sieck, M.G. Tay, M.-H. Thibault, R.M. Edkins, K. Costuas, J.-F. Halet, A.S. Batsanov, M. Haehnel, K. Edkins, A. Lorbach, A. Steffen, T.B. Marder, Reductive Coupling of Diynes at Rhodium Gives Fluorescent Rhodacyclopentadienes or Phosphorescent Rhodium 2,2′-Biphenyl Complexes, Chem. Eur. J. 22 (2016) 10523–10532. https://doi.org/10.1002/chem.201601912.; b) A. Steffen, R.M. Ward, M.G. Tay, R.M. Edkins, F. Seeler, M. van Leeuwen, L.-O. Pålsson, A. Beeby, A.S. Batsanov, J.A.K. Howard, T.B. Marder, Regiospecfic Formation and Unusual Optical Properties of 2,5-Bis(arylethynyl)rhodacyclopentadienes: A New Class of Luminescent Organometallics, Chem. Eur. J. 20 (2014) 3652–3666. https://doi.org/10.1002/chem.201304068.; c) A. Steffen, K. Costuas, A. Boucekkine, M.-H. Thibault, A. Beeby, A.S. Batsanov, A. Charaf-Eddin, D. Jacquemin, J.-F. Halet, T.B. Marder, Fluorescence in Rhoda- and Iridacyclopentadienes Neglecting the Spin-Orbit Coupling of the Heavy Atom: The Ligand Dominates, Inorg. Chem., 53 (2014) 7055–7069. https://doi.org/10.1021/ic501115k.; d) A. Steffen, M.G. Tay, A.S. Batsanov, J.A.K. Howard, A. Beeby, K.Q. Vuong, X.-Z. Sun, M.W. George, T.B. Marder, 2,5-Bis(p-Arylethynyl)-Rhodacyclopentadienes Show Intense Fluorescence: Denying the Presence of a Heavy Atom, Angew. Chem. Int. Ed., 49 (2010) 2349–2353. https://doi.org/10.1002/anie.200905697.; e) J.P. Rourke, A.S. Batsanov, J.A.K. Howard, T.B. Marder, Regiospecific High Yield Reductive Coupling of Diynes to Give a Luminescent Rhodium Complex, Chem. Commun. (2001) 2626–2627. https://doi.org/10.1039/B108625A.

[31] a) J. Lewis, M.S. Khan, A.K. Kakkar, B.F.G. Johnson, T.B. Marder, H.B. Fyfe, F. Wittmann, R.H. Friend, A.E. Dray, Di-, Tri-, Pseudo-di, and Pseudo-tetra-acetylenic Polymers of Platinum: Synthesis, Characterization, and Optical Spectra, J. Organometal. Chem. 425 (1992) 165–176. https://doi.org/10.1016/0022-328X (92)80033-T.; b) T.B. Marder, G. Lesley, Z. Yuan, H.B. Fyfe, P. Chow, G. Stringer, I. R. Jobe, N.J. Taylor, I.D. Williams, S.K. Kurtz, Transition Metal Acetylides for Nonlinear Optics, in: S.R. Marder, J. Sohn, G.D. Stucky (Eds.), Materials for Nonlinear Optics: Chemical Perspectives, ACS Symposium Series, 1991, pp. 605–615.; c) H.B. Fyfe, M. Mlekuz, D. Zargarian, N.J. Taylor, T.B. Marder, Synthesis of Mononuclear, Dinuclear, and Oligomeric Rigid-Rod Acetylide Complexes of Rhodium and the Molecular Structure of [Rh(PMe3)4{-C≡C-p-C6H4- C≡C-)Rh(PMe3)4], J. Chem. Soc., Chem. Commun. (1991) 188–190. https://doi.org/10.1039/C39910000188.

[32] S.M. Berger, M. Ferger, T.B. Marder, Synthetic Approaches to Triarylboranes from 1885 to 2020, Chem. Eur. J. 27 (2021) 7043–7058, https://doi.org/10.1002/chem.202005302.

[33] S.M. Berger, T.B. Marder, Applications of triarylborane materials in cell imaging and sensing of bio-relevant molecules such as DNA, RNA, and proteins, Mater. Horiz. 9 (2022) 112–120, https://doi.org/10.1039/D1MH00696G.

[34] a) C.D. Entwistle, T.B. Marder, Applications of three-coordinate organoboron compounds and polymers in optoelectronics, Chem. Mater. 16 (2004) 4574–4585. https://doi.org/10.1021/cm0495717; b) C.D. Entwistle, T.B Marder, Boron Chemistry Lights the Way: Optical Properties of Molecular and Polymeric Systems, Angew. Chem. Int. Ed. Engl. 41 (2002) 2927–2931. https://doi.org/10.1002/1521-3773(20020816)41:16<2927::AID-ANIE2927>3.0.CO;2-L.

[35] Z.M. Hudson, S. Wang, Metal-containing triarylboron compounds for optoelectronic applications, Dalton Trans. 40 (2011) 7805–7816, https://doi.org/10.1039/C1DT10292C.

[36] G. Turkoglu, M.E. Cinar, T. Ozturk, Triarylborane-based materials for OLED applications, Molecules 22 (2017) 1522, https://doi.org/10.3390/molecules22091522.

[37] L. Ji, S. Griesbeck, T.B. Marder, Recent Developments in and Perspectives on Three-Coordinate Boron Materials: A Bright Future, Chem. Sci. 8 (2017) 846–863, https://doi.org/10.1039/C6SC04245G.

[38] Z.-B. Sun, S.-Y. Li, Z.-Q. Liu, C.-H. Zhao, Triarylborane π-electron systems with intramolecular charge-transfer transitions, Chin. Chem. Lett. 27 (2016) 1131–1138, https://doi.org/10.1016/j.cclet.2016.06.007.

[39] J.C. Doty, B. Babb, P.J. Grisdale, M. Glogowski, J.L.R. Williams, Boron photochemistry: IX. Synthesis and fluorescent properties of dimesityl-phenylboranes, J. Organomet. Chem. 38 (1972) 229–236, https://doi.org/10.1016/S0022-328X(00)83321-5.

[40] C.-W. Chiu, Y. Kim, F.P. Gabbaï, Lewis acidity enhancement of triarylboranes via peripheral decoration with cationic groups, J. Am. Chem. Soc. 131 (2009) 60–61, https://doi.org/10.1021/ja808572t.

[41] S.M. Berger, J. Rühe, J. Schwarzmann, A. Phillipps, A.K. Richard, M. Ferger, I. Krummenacher, L.M. Tumir, Z˝. Ban, I. Crnolatac, D. Majhen, I. Bariˇsi´c, I. Piantanida, D. Schleier, S. Griesbeck, A. Friedrich, H. Braunschweig, T.B. Marder, Bithiophene-Cored, mono-, bis-, and tris-(Trimethylammonium)-Substituted, bis-Triarylborane Chromophores: Effect of the Number and Position of Charges on Cell Imaging and DNA/RNA Sensing, Chem. Eur. J. 27 (2021) 14057–14072, https://doi.org/10.1002/chem.202102308.

[42] S. Griesbeck, M. Ferger, C. Czernetzi, C. Wang, R. Bertermann, A. Friedrich, M. Haehnel, D. Sieh, M. Taki, S. Yamaguchi, T.B. Marder, Optimization of Aqueous Stability versus π-Conjugation in Tetracationic Bis(triarylborane) Chromophores: Applications in Live-Cell Fluorescence Imaging, Chem. Eur. J. 25 (2019) 7679–7688, https://doi.org/10.1002/chem.201900723.

[43] G.-L. Fu, H. Pan, Y.-H. Zhao, C.-H. Zhao, Solid-state emissive triarylborane-based BODIPY dyes: Photophysical properties and fluorescent sensing for fluoride and cyanide ions, Org. Biomol. Chem. 9 (2011) 8141–8146, https://doi.org/10.1039/C1OB05959A.

[44] C. Yao, Z. Tian, D. Jin, F. Zhao, Y. Sun, X. Yang, G. Zhou, W.-Y. Wong, Platinum(II) acetylide complexes with star-and V-shaped configurations possessing good trade-off between optical transparency and optical power limiting performance, J. Mater. Chem. C 5 (2017) 11672–11682, https://doi.org/10.1039/C7TC03542J.

[45] S.-T. Lam, N. Zhu, V.-W.-W. Yam, Synthesis and characterization of luminescent rhenium(I) tricarbonyl diimine complexes with a triarylboron moiety and the study of their fluoride ion-binding properties, Inorg. Chem. 48 (2009) 9664–9670, https://doi.org/10.1021/ic900803a.

[46] M. Ferger, Z˝. Ban, I. Kroˇsl, S. Tomi´c, L. Dietrich, S. Lorenzen, F. Rauch, D. Sieh, A. Friedrich, S. Griesbeck, A. Kenđel, S. Miljani´c, I. Piantanida, T.B. Marder, Bis(phenylethynyl)arene Linkers in Tetracationic Bis-triarylborane Chromophores Control Fluorimetric and Raman Sensing of Various DNAs and RNAs, Chem. Eur. J. 27 (2021) 5142–5159, https://doi.org/10.1002/chem.202005141.

[47] Z˝. Ban, S. Griesbeck, S. Tomi´c, J. Nitsch, T.B. Marder, I. Piantanida, A quadrupolar bis-triarylborane chromophore as a fluorimetric and chirooptic probe for simultaneous and selective sensing of DNA, RNA and proteins, Chem. Eur. J. 26 (2020) 2195–2203, https://doi.org/10.1002/chem.201903936.

[48] M. Demeunynck, C. Bailly, W.D. Wilson, Small molecule DNA and RNA binders: from synthesis to nucleic acid complexes, John Wiley & Sons, Weinheim, 2006.

[49] J. Langer, D. Jimenez de Aberasturi, J. Aizpurua, R.A. Alvarez-Puebla, B. Auguí´e, J. J. Baumberg, G.C. Bazan, S.E. Bell, A. Boisen, A.G. Brolo, Present and future of

surface-enhanced Raman scattering, ACS Nano 14 (2019) 28–117, https://doi.org/10.1021/acsnano.9b04224.

[50] D. Cialla, S. Pollok, C. Steinbrücker, K. Weber, J. Popp, SERS-based detection of biomolecules, Nanophotonics 3 (2014) 383–411, https://doi.org/10.1515/nanoph-2013-0024.

[51] F. Hu, C. Zeng, R. Long, Y. Miao, L. Wei, Q. Xu, W. Min, Supermultiplexed optical imaging and barcoding with engineered polyynes, Nat. Meth. 15 (2018) 194–200, https://doi.org/10.1038/nmeth.4578.

[52] M. Tommasini, A. Milani, D. Fazzi, A. Lucotti, C. Castiglioni, J.A. Januszewski, D. Wendinger, R.R. Tykwinski, π-conjugation and end group effects in long cumulenes: Raman spectroscopy and DFT calculations, J. Phys. Chem. C 118 (2014) 26415–26425, https://doi.org/10.1021/jp509724d.

[53] L.M. Tumir, I. Piantanida, I.J. Cindri´c, T. Hrenar, Z. Mei´c, M. Z˘ini´c, New Permanently Charged Phenanthridinium-Nucleobase Conjugates. Interactions with Nucleotides and Polynucleotides and Recognition of ds-PolyAH, J. Phys. Org. Chem. 16 (2003) 891–899, https://doi.org/10.1002/poc.680.

[54] C.H. Munro, W.E. Smith, M. Garner, J. Clarkson, P.C. White, Characterization of the Surface of a Citrate-Reduced Colloid Optimized for Use as a Substrate for Surface-Enhanced Resonance Raman Scattering, Langmuir 11 (10) (1995) 3712–3720, https://doi.org/10.1021/la00010a021.

[55] T. Mosmann, Rapid colorimetric assay for cellular growth and survival: Application to proliferation and cytotoxicity assays, J. Immunol. Methods 65 (1983) 55–63, https://doi.org/10.1016/0022-1759(83)90303-4.

[56] T.M. Schnabel, D. Melcher, K. Brandhorst, D. Bockfeld, M. Tamm, Unraveling the Mechanism of 1,3-Diyne Cross-Metathesis Catalyzed by Silanolate-Supported Tungsten Alkylidyne Complexes, Chem. Eur. J. 24 (2018) 9022–9032, https://doi.org/10.1002/chem.201801651.

[57] J. Heppekausen, R. Stade, A. Kondoh, G. Seidel, R. Goddard, A. Fürstner, Chem. Eur. J. 18 (2012) 10281–10299, https://doi.org/10.1002/chem.201200621.

[58] S. Lysenko, J. Volbeda, P.G. Jones, M. Tamm, Catalytic Metathesis of Conjugated Diynes, Angew. Chem. Int. Ed. 51 (2012) 6757–6761, https://doi.org/10.1002/anie.201202101.

[59] A. Fürstner, Alkyne Metathesis on the Rise, Angew. Chem. Int. Ed. 52 (2013) 2794–2819, https://doi.org/10.1002/anie.201204513.

[60] J.D. McGhee, P.H.V. Hippel, Theoretical Aspects of DNA-Protein Interactions - Cooperative and Non-Cooperative Binding of Large Ligands to a One-Dimensional Homogeneous Lattice, J. Mol. Biol. 86 (1974) 469–489, https://doi.org/10.1016/0022-2836(74)90031-X.

[61] A. Rodger, B. Norden, Circular dichroism of biomolecules, in: A. Rodger, B. Norden, Circular Dichroism and Linear Dichroism, Oxford University Press, New York, 1997, pp. 15–31.

[62] T. S˘midlehner, I. Piantanida, G. Pescitelli, Polarization spectroscopy methods in the determination of interactions of small molecules with nucleic acids - tutorial, Beilstein J. Org. Chem. 14 (2018) 84–105, https://doi.org/10.3762/bjoc.14.5.

[63] J.-L. Mergny, L. Lacroix, Analysis of Thermal Melting Curves, Oligonucleotides 13 (2003) 515–537, https://doi.org/10.1089/154545703322860825.

[64] H. Amini, Z˘. Ban, M. Ferger, S. Lorenzen, F. Rauch, A. Friedrich, I. Crnolatac, A. Kenđel, S. Miljani´c, I. Piantanida, T.B. Marder, Tetracationic Bis-Triarylborane 1,3-Butadiyne as a Combined Fluorimetric and Raman Probe for Simultaneous and Selective Sensing of Various DNA, RNA, and Proteins, Chem. Eur. J. 26 (2020) 6017–6028, https://doi.org/10.1002/chem.201905328.